

Foot Pressure from Video: A Deep Learning Approach to Predict Dynamics from Kinematics

Savinay Nagendra, Christopher Funk, Robert T. Collins, Yanxi Liu

Lab for Perception, Action and Cognition

Department of Computer Science and Engineering, The Pennsylvania State University, USA

Abstract

Human gait stability analysis is a key to understanding locomotion and control of body equilibrium, with numerous applications in the fields of Kinesiology, Medicine and Robotics. This work introduces a novel approach to learn dynamics of a human body from kinematics to aid stability analysis. We propose an end-to-end deep learning architecture to regress foot pressure from a human pose derived from video. This approach utilizes human Body-25 joints extracted from videos of subjects performing choreographed Taiji (Tai Chi) sequences using OpenPose estimation. The derived human pose data and corresponding foot pressure maps are used to train a convolutional neural network with residual architecture, termed “PressNET”, in an end-to-end fashion to predict the foot pressure corresponding to a given human pose. We create the largest dataset for simultaneous video and foot pressure on five subjects containing >350k frames. We perform cross-subject evaluation with data from the five subjects on two versions of PressNET to evaluate the performance of our networks. K-Nearest Neighbors (KNN) is used to establish a baseline for comparisons and evaluation. We empirically show that PressNet significantly outperform KNN on all the splits.

1. Introduction

In the realm of health and sports, precise and quantitative digital recording of human motion and analysis provide rich content for performance characterization and training, cross-sectional/longitudinal health status assessment and diagnosis or even preventive therapy of neurodegenerative syndromes. In recent years, gait analysis and control/balance of equilibrium has received an increasing interest from the research community. This is mainly due to the necessity of understanding the complex mechanisms of the human postural system, which contribute to the development of efficient solutions for unstable postures in terms of orientation and equilibrium. Stability analysis has a wide

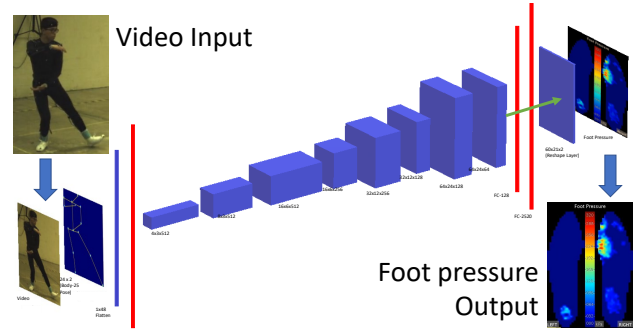


Figure 1. Our PressNET networks to predict foot pressure heatmap from video based on extracting Body-25 joints from a video frame using OpenPose estimation and regressing directly to foot pressure. The green line signifies a skip connection around the non-local fully connected layers.

number of applications in fields of Health care, Kinesiology and Robotics, aiming to understand locomotion and duplicate human body movements during numerous physical activities. Understanding body dynamics, such as foot pressure, is essential to study the effects of perturbations caused by external forces and torques on the human postural system, which changes body equilibrium in static posture as well as during locomotion.

Current computer vision research focuses mainly on extracting skeletal kinematics from videos, using body pose estimation and tracking to infer an estimate of skeletal pose and joint angles in each frame as well as the movement of body and limbs over time [2,5,6,7,8,9,12,16,35,48]. However, little has been investigated on whether quantitative dynamics information can be inferred from a single video of a person’s movement. While body joints and their degrees of freedom constrain the types of motion, it is the properties and actions of the muscles and weight distributions, i.e. body dynamics, that dictate the range of motion, speed and feasible poses produced with these degrees of freedom. Consideration of human body dynamics has been successful in explaining performance in athletics activities, for example the triple jump [2], and vertical jump performance [11].

Similarly, analysis of dynamics has been used to show that strength is the limiting factor in the ability of the elderly to rise from a chair [22], and to determine the causes of stiff-knee gait in subjects with cerebral palsy [13]. We believe an effective analysis of human movement must take into account the the dynamics of the human body, and we ask the question: Can human motion dynamics be inferred from video sensors that are incapable of observing muscle activations, physical loads and external forces directly?

This paper explores a deep learning approach to transform kinematics (body pose) to dynamics (foot pressure). In order to achieve this goal, we have created the largest dataset with over 350k frames of synchronized video and foot pressure. We represent foot pressure by an intensity heatmap that provides the distribution of pressure applied by different points of the foot against the ground, measured in kilo Pascals (kPa) over discretized foot sole locations. The body pose is represented in terms of human Body-25 joint locations, extracted from videos of subjects performing choreographed Taiji (Tai Chi) sequences by applying Openpose on the video frames. For training data, we record video data and foot pressure maps synchronously so that there is a foot pressure map of both feet corresponding to each video frame. This is used as training data to train two versions of a deep convolutional neural network residual architecture to regress foot pressure heatmaps from a given body pose. We perform a leave-one-out cross subject evaluation over the data of five subjects using our network. K-Nearest Neighbors (KNN) is applied to establish a baseline for each of the five cross-subject splits. Mean absolute error is used to evaluate the performance of the networks. Our results show that the network out-performs KNN across all the five splits.

We present a method to predict foot pressure heatmaps directly from video alone and the major contributions of this paper are:

- We present a novel deep architecture, PressNET, which is the first network to regress foot pressure of a subject directly from video, aiding in human gait stability analysis
- This is the first paper to successfully achieve domain transformation between kinematics (human pose) and dynamics (foot pressure) using deep learning on our new dataset
- We create the largest synchronized video and foot pressure dataset ever recorded.

2. Related Work

After the introduction of Deep Pose by Toshev *et al.* [4], there was a paradigm shift in the field of human pose estimation from classical approaches to deep networks. The idea of using heatmaps for visualization [4] as well as for use as ground truth data in a regression problem was intro-

duced for the first time by Thompson *et al.* [47]. Stacked hour glass networks by Newell *et al.* [35] gave state of the art results for pose estimation using heat map regression with a bottom-up top-down approach. They use the network based off Thompson *et al.*, where convolution layers are used jointly with a graphical model to learn spatial relationships between joints and other human pose estimators [1,18,25,30,31,32,36,38,40,41,42,43,44,45,46,52,53]. This was the first network to successfully implement a pose estimator using residual convolution layers for additional spatial processing at different resolutions. Encoder-Decoder architectures have been predominantly used for human pose estimation. An hourglass network, before stacking, is also similar to an encoder-decoder architecture, where skip connections help in preserving spatial coherence at each scale [4]. Having deep residual/skip connections to preserve spatial information across multiple resolutions through the network is essential for unsupervised/semi-supervised feature learning [51]. Densely connected convolutional networks have achieved state of the art accuracies by using residual feed forward connections between convolution layers.

Success in 2D human pose estimations has encouraged researchers to detect 3D skeletons from image/video by extending the existing 2D human pose detectors [3,27] or by directly using the image features [1,32,36,44]. State-of-the-art methods for 3D human pose estimation from 2D images have concentrated on deep systems. Tome *et al.* [46] proposed an estimator that reasons about 2D and 3D estimation to improve both tasks. Zhou *et al.* [40,52] augmented a 2D estimator with a 3D depth regression sub-network. Martinez *et al.* [31] showed that given high-quality 2D joint information, the process of lifting 2D pose to 3D pose can be done efficiently using a relatively simple deep feed-forward network.

Until now all the papers discussed concentrate on pose estimation from 2D images or depth maps. These papers concentrate on learning joint angles or joint locations, which can be broadly classified as learning a very basic type of kinematics for a whole body skeleton. These methods do not delve into the external torque/force exerted by the environment which lead to a change in balance or physical interaction of the body with the scene.

There have been a many studies on human gait analysis using qualitative approaches. Lee *et al.* [30] aimed to predict the pose of a patient using foot pressure mats. Mrozowski *et al.* [33] used frieze patterns to analyze gait sequences [10,15,19,20,24,37,39,49]. Although these are some insightful ways to analyze gait stability, there has been no deep learning approach to tackle this problem. In this paper, we aim to use body kinematics to predict its dynamics and hence deduce a quantitative method to achieve gait stability analysis using foot pressure.

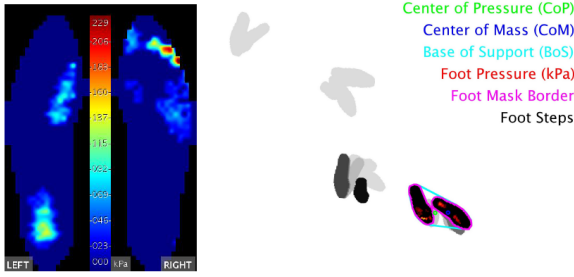


Figure 2. Example frame from Subject 4, Session 1, Take 2 showing left and right foot pressure color coded based on maximum pressure (kPa), with foot pressure sequences spatiotemporally registered to the motion capture coordinate system.

3. Our Approach

3.1. Data Collection

Three modes of data - Video, Motion Capture and Foot pressure are recorded simultaneously for five subjects performing choreographed 24-Form Taiji-Quan sequences. Each session consists of three performances by the subject with an outfit consisting of motion capture markers and insole pressure measurement sensors. Vicon Nexus software has been used to synchronize motion capture and video data spatio-temporally, while Tekscan F-scan foot pressure sensor measurements are synchronized post collection. This is the first dataset to record synchronized video, motion capture and foot pressure data.

3.1.1 Video

Raw video data is processed using the Nexus software to trans-code it to a compressed video, with each video having its own spatio-temporal calibration. This compressed video is then processed using OpenPose [6]. OpenPose uses non-parametric representations, referred to as Part Affinity Fields, to regress joint positions as well as connections between the joints. We use the maximum accuracy configuration of the network to extract Body-25 joints from videos. Each detected key-point has a confidence associated with it, which determines the accuracy of prediction of a particular joint location. The output from OpenPose network has 3 channels - (X, Y, confidence), denoting the X and Y pixel coordinates and confidence of prediction for each of the 25 joints, making it of size (25×3) .

Figure 10 shows the body-25 skeleton. The 25 keypoints are: {0:Nose, 1:Neck, 2:RShoulder, 3:RElbow, 4:RWrist, 5:LShoulder, 6:LElbow, 7:LWrist, 8:MidHip, 9:RHip, 10:RKnee, 11:RAnkle, 12:LHip, 13:LKnee, 14:LAnkle, 15:REye, 16:LEye, 17:REar, 18:LEar, 19:LBigToe, 20:LSmallToe, 21:LHeel, 22:RBigToe, 23:RSmallToe, 24:RHeel} The video frames of a subject performing Tai Chi, as shown in Figure 10 are processed through the Open-

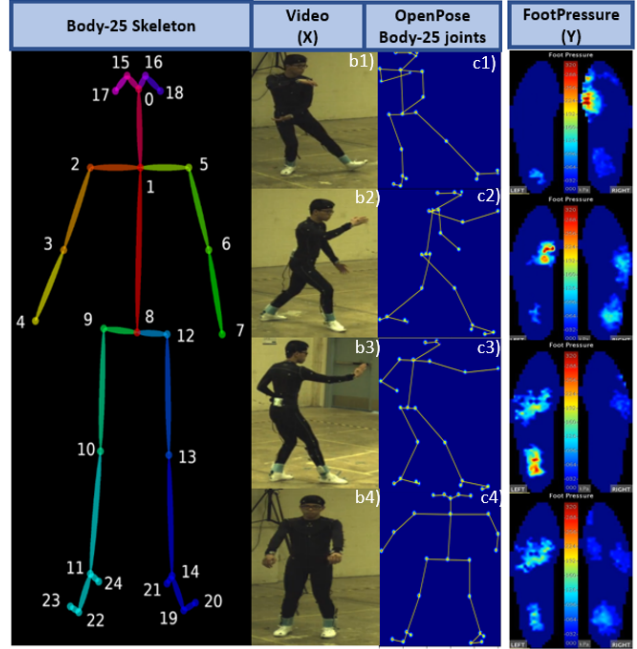


Figure 3. Left: Body-25 joint set labeled by Openpose. Middle: The video data and the corresponding Openpose detections showing the detected skeletons with Gaussian distributions over each joint. The 2D position of these joints are used as the input to the PressNETs. Right: the corresponding foot pressure which the PressNETs are trained to output.

Pose network to extract the above mentioned 25 body joint locations with respect to a fixed coordinate axis. For the purpose of visualization, 2D Gaussian heatmaps are drawn over the joint locations, with the peak of each Gaussian corresponding to the confidence of detection of that joint, as shown in Figure 10. The confidence of keypoints 15 to 18 are zero for more than 50% of the video frames due to occlusions. However, these keypoints are still given as inputs to our network. The reason for this is as follows: We are trying to establish a correlation between the 25 key points and the corresponding foot pressures where we want our network to learn the factor of usability of each key point in predicting the foot pressure without prior assumptions as to which key points might be necessary in the regression task. Eventually, the network learns to discard the zero confidence key points to avoid affecting the accuracy of prediction.

3.1.2 Foot Pressure

Foot pressure is collected using a Tekscan F-Scan insole pressure measurement system. Each subject was provided a pair of canvas shoes outfitted with cut to fit capacitive pressure measurement insoles that have a maximum width of 21 prexels (pressure pixels) and a maximum height of 60 prexels with a total of approximately 900-1,000 pressure

Subject	Session	Take	# frames	Foot Pressure Statistics (kilo Pascals)					Total # frames
				Mean	Std	Median	Max	Min	
Subject-4	1	1	9,595	6.52	10.62	1.99	73.12	0	99,609
		2	14,364	6.24	10.16	1.91	74.32	0	
		3	2,412	5.94	8.94	2.67	55.33	0	
	2	1	14,248	7.74	12.866	2.27	99.57	0	
		2	13,460	8.41	14.28	2.33	110.95	0	
		3	13,255	8.87	15.13	2.29	117.92	0	
	3	1	5,917	6.47	10.46	2.16	63.78	0	
		2	13,106	6.38	11.22	1.86	88.36	0	
		3	13,252	6.44	11.05	1.87	78.64	0	
Subject-7	1	1	18,000	3.37	4.72	2.4	31.33	0	158,920
		2	17,626	3.47	4.45	2.18	28.5	0	
		3	17,702	3.29	4.27	2.08	28.98	0	
	2	1	17,706	6.18	8.09	3.79	56.95	0	
		2	17,354	5.76	7.74	3.53	55.47	0	
		3	17,625	5.42	7.43	3.25	53.85	0	
	3	1	17,576	5.4	8.04	2.98	62.45	0	
		2	17,645	5.39	7.94	3.09	62.4	0	
		3	17,686	5.35	8.12	2.91	62.07	0	
Subject-8	2	1	14,103	5.26	11.84	0.069	99.05	0	19,702
	3	1	5,599	2.94	7.43	0.027	56.15	0	
Subject-9	1	1	11,211	4.4	6.942	1.37	51.52	0	34,915
	2	1	11,294	6.15	11.19	1.34	89.93	0	
	3	1	12,410	5.78	11.91	0.96	106.18	0	
Subject-10	1	1	13,064	7.35	11.07	2.53	82.68	0	41,871
	2	1	14,500	8.27	14.39	1.94	125.97	0	
	3	1	14,307	8.04	14.82	1.2	124.07	0	

Table 1. Data statistics showing number of video frames per take and session for each subject.

prexels depending on shoe size. These two insole sensors are recorded through a battery operated wearable recording system. The data is recorded with a noise floor of approximately 3kPa.

During each session, the subject follows an integrated calibration process that determines a linear (scale and offset) calibration for all active prexels of each foot sensor. Each take is then recorded as a 36,000 sample series (100 Hz for 6 minutes) that is logged and then downloaded at the end of the session. Each take of the raw foot pressure data is subject to issues including non-responsive (bad) prexels and measurement noise. To mitigate these issues, a median filter is applied temporally to remove impulse noise using an 11 frame median filter and we use a 3x3 filter (or 5x3 filter for bad prexel regions larger 1x1) within each frame to remove the noise spatially. The foot pressure heatmaps generated are 2 channel images of size 60×21 .

Figure 10 shows an example of left and right foot pressure visualized with a color mapping (left) and registered into the spatial coordinates of the motion capture system (right).

3.1.3 Data Statistics

Data from five subjects performing choreographed sequences of 24-Form Taiji Quan sequences has been used for all experiments in this paper. The entire dataset contains over 350k frames of data with video and foot pressure data for each frame. The five subjects are named : {‘Subject-4’, ‘Subject-7’, ‘Subject-8’, ‘Subject-9’ and ‘Subject-10’}. The mean, median, standard deviation, maximum and minimum foot pressure values in kilo pascals for each take is shown in Table 1. The sizes of each data split are shown in Table 2. Nine takes of subjects 4 and 7 over 3 sessions are

used. This is the largest video+foot pressure dataset ever created and will be released on acceptance of this paper.

3.2. Network and Training

The design of our network is loosely motivated by the residual generator of the Improved Wasserstein GAN [14, 17]. We are using a generator inspired architecture since our input is 1D, converted to a 2D heatmap. This design aids in capturing information at different resolutions, acting like a decoder network for feature extraction. The primary aim of our network is to extract features without loss of spatial information across different resolutions. The idea of our design is analogous to generating images using a flattened noise vector. Here, we try to learn the correlation between the pose encoded in terms of 25 joint locations and the corresponding foot pressure intensity distribution. We train a convolutional residual architecture over data from multiple subjects to regress foot pressure distributions given a pose. We do not use a discriminator since ground truth data is available and the problem is supervised.

3.2.1 Data Pre-processing

Input Pose data is centered around the hip joint to aid the network in generalizing to different subjects and to remove camera specific constraints of video recording. The hip joint, which is (0,0) after centering, is removed from the data set. Data is subjected to per-feature normalization by subtracting each feature by its mean and dividing by its standard deviation. Zero confidence OpenPose joints are not considered when the mean and standard deviation are calculated.

Foot pressure data, which is originally recorded in kilo Pascals (kPa) has invalid prexels representing regions outside the footmask marked as Not a Number (nan). These prexels are converted to zeros. Any pressure prexel values greater than 1000 kilopascals are clipped to 1000 to remove noise from the dataset. The data is converted to Mega Pascals by dividing by 1000, so that the intensities are in the range $[0, 1]$.

3.3. Network

The input layer is a flattened vector of joint coordinates of size 48×1 (24 joints \times 2 coordinates since the hip joint is removed), which has the kinematic information about a pose. The input is processed through a fully connected layer with an output dimension of 6144×1 . This output is reshaped into an image of size 4×3 with 512 channels. The network must have some mechanisms to effectively upsample and calculate features across scales. For this purpose, we use four residual convolution blocks which use nearest neighbor upsampling and then compute activations at each scale. A residual block is shown in Figure 4 Right. The first

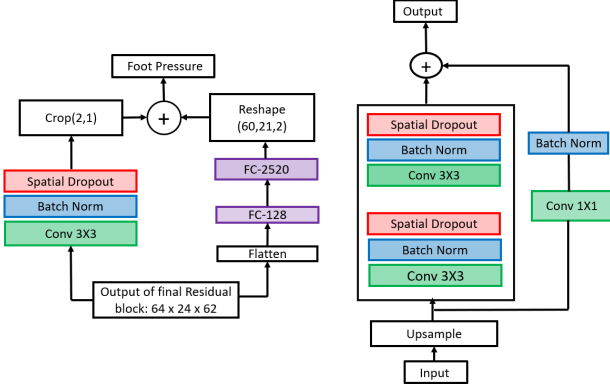


Figure 4. Left: Residual output Block of our network with a Fully connected layers to maintain spatial consistency. Right: Residual block, which are building blocks of our network.

block upsamples the input by (2, 1) and the other three upsample by 2. Each block has two convolution layers of kernel size 3×3 . The input to each block is passed through a 1×1 convolution block and added as a residual connection to the output of the block. This ensures a pipeline to preserve spatial information at multiple resolutions. The resolution of each block is progressively halved, starting at 512 channels and decreasing to 64. The output of the final residual block is flattened and fed into a fully connected layer FC-128. The final output from the last residual block is also passed into a 3×3 convolution layer to get a 2 channel output of shape 64×24 . This output is further cropped to obtain a two-channeled image of shape $60 \times 21 \times 2$, which is the shape of the foot pressure heatmaps. This output is added to the final FC-2520 layer as a residual connection to preserve spatial coherence even after passing through flattening and dense layers. The last residual fully connected block of our architecture is motivated loosely by the idea of Non-Local Neural Networks [12]. We call this architecture “PressNET-V2”. Another variant, “PressNET-V1”, has no residual connection in the output block. This network processes 1D-2D-1D, where the residual blocks work as feature extractors and the features are fed into fully connected layers. This block is shown in Figure 4. The pipeline of this project and the resolution change through the network architecture is portrayed in Figure 6. We use depth-wise separable convolution layers in every block to ensure that spatial coherence is preserved with changes in resolution. Since separable convolution layers split a kernel into two to perform depth-wise and point-wise convolutions, the number of parameters of the network are also reduced, thus reducing training time. Batch normalization [23] and spatial dropouts are applied after every convolution layer. ReLU [34] is used as a common activation function throughout the network, except the output layer.

Test Subject	Training Set	Validation Set	Test Set
4	206,406	50,002	99,609
7	213,051	45,568	158,920
8	277,660	57,655	19,702
9	269,258	508,44	34,915
10	264,199	48,947	41,871

Table 2. The number of frames in each split of the data.

3.3.1 Training Details

We evaluate the two varieties of our network on five splits of the dataset. Our dataset is split by subject in a leave-one-out fashion, where four subjects are used for training and we test on the fifth. The validation data consists of the last take from each subject used in the training data. The validation data is about 7% to 10% of training data depending on the data split being used. The number of frames per take are listed in Table 1. The goal of this cross-subject validation is to show how well this network generalizes to an unseen individual. Both networks are trained with a learning rate of $5e^{-5}$ for 20 epochs at a batch size of 32 for all splits on a NVIDIA Tesla P100 GPU cluster with 8GB of memory. Data pre-processing is carried out before training as mentioned in Section 3.2.1. Both PressNet-V1 and PressNet-V2 take 3 to 3.5 hours to train on splits with test subjects 8, 9 and 10 and 2 to 2.5 hours to train on splits with test subjects 4 and 7. The problem is formulated as a regression with a sigmoid activation layer as the last activation layer since the output data is in the range $[0, 1]$. A binary footmask is elementwise multiplied in the network having ones marked for valid prexels and zeros marked for invalid prexels. This enables the network to not have to learn the approximate shape of the foot in the course of training and solely learn foot pressure. The learning rate is reduced to $1e^{-5}$ after 12 epochs to ensure a decrease in validation loss with training. Mean absolute error is used as the loss function for supervision, as we are learning the distribution of prexels [3].

4. Results

We evaluate PressNET exhaustively both qualitatively and quantitatively as well as compare against a K-nearest neighbor baseline to show that PressNET is effective at estimating foot pressure.

KNN Baseline

In order to compare the accuracy of our networks against another type of regression, we employ K-Nearest Neighbor (KNN) regression [?] as a baseline. For the KNN regression, the data is temporally subsampled by a factor of 2. This is done to decrease the search time required for the KNN algorithm, but without losing much information. The

foot pressure data is sampled at 100Hz, i.e., we have a frame of foot pressure recorded every 10 milliseconds. Since the data is sequential, picking every other frame of training data does not affect the temporal consistency of foot pressure data as the change in the heatmaps in 20 milliseconds is negligible. Pre-processing is carried out similar to training PressNet. The data is normalized by mean and standard deviation of input, calculated using hip joint centered data by ignoring zero confidence values. The distance metric for the KNN algorithm is calculated as the mean of the distances between joints which do not have zero confidence values. This distance d can be represented for two OpenPose human pose detections (a and b) with confidence c^a for a and c^b for b and J joints by:

$$d(x, y) = \frac{\sum_{i \in J} \|a_i - b_i\|_2^2 * \delta(c_i^a * c_i^b > 0)}{\sum_{i \in J} \delta(c_i^a * c_i^b > 0)} \quad (1)$$

where δ is the Kronecker Delta which is 1 if the argument is true and 0 if false. This enables KNN to adapt to missing joint detections in the human pose predictions.

4.1. Quantitative Results

For the quantitative evaluation, we use mean absolute error E to quantify the difference between ground truth foot pressure Y predicted foot pressure \hat{Y} on N foot pressure prexels as:

$$E = \frac{1}{|N|} \sum_{n \in N} |Y_n - \hat{Y}_n|. \quad (2)$$

We then take the mean across all the cross-validation splits for our final accuracy rates.

Table 3 shows the error for our PressNET and the KNN error for the predicted foot pressure for each data split. For both PressNETs, the worst two individuals to predict foot pressure on are Subjects 4 and 8. This is also true for the nearest neighbor classifiers as well which could be because these subject foot pressures have a higher mean foot pressure than the other subjects and thus the networks are underpredicting the error. The PressNET V2 has a mean classification of 5.61 kPa which is less than double the 3 kPa noise floor of the foot pressure recording devices.

In order to test whether these results are significant, we perform a two tailed paired t-test between the mean errors for each frame for each of the PressNETs compared with KNN over each split of the data. As shown in Table 4, both networks perform significantly better than KNN regression.

4.2. Qualitative Results

Figure 5 shows the foot pressure predictions for different frames from multiple subjects. In addition to the qualitative comparison by visualization, the respective mean absolute errors with respect to ground truth frames have also been

KNN		Testing Mean Absolute Errors (kPa)			
Test Subject	Mean	Std	Median	Max	Min
4	11.37	2.67	9.95	23.92	3.91
7	9.97	2.4	8.97	22.6	3.007
8	9.73	2.6	8.8	19.21	3.08
9	9.95	2.89	9.32	23.12	2.86
10	11.43	3.08	10.01	25.01	3.51
Means	10.49	2.73	9.41	22.78	3.28
PressNET V1		Testing Mean Absolute Errors (kPa)			
Test Subject	Mean	Std	Median	Max	Min
4	8.22	2.12	8.08	19.43	2.38
7	5.47	1.78	5.21	19.28	2.18
8	5.74	2.13	5.51	18.32	0.82
9	5.59	1.87	5.23	17.16	1.28
10	8.76	2.31	8.38	22.22	3.47
Means	6.76	2.04	6.48	19.28	2.02
PressNET V2		Testing Mean Absolute Errors (kPa)			
Test Subject	Mean	Std	Median	Max	Min
4	6.97	1.97	6.85	18.02	2.39
7	4.67	1.86	4.37	17.29	2.3
8	4.63	2.03	4.46	17.1	0.69
9	4.6	1.907	4.24	19.15	1.19
10	7.21	2.28	7.35	21.06	3.165
Means	5.61	2.009	5.45	18.52	1.94

Table 3. Results for KNN and PressNET V1 and V2 showing the mean absolute error for each split of the data and the mean among the splits. For every statistic, PressNET V2 has the lowest error out of all the regressions tested. The lowest mean values are shown in bold.

Test Subject	PressNET-V1		PressNET-V2	
	t-statistic	P-value	t-statistic	P-value
4	298.19	0	352.13	0
7	597.7	0	548.53	0
8	178.69	0	191.75	0
9	261.84	0	260.87	0
10	106.76	0	111.55	0

Table 4. Paired t-test between Mean Absolute errors of all frames between PressNET-V1, PressNET-V2 and KNN

calculated to provide a quantitative comparison of performance of the three networks. The frames have been chosen to show the ability of PressNet to generalize to different poses, similar poses from different subjects and different views with respect to a fixed camera. The frames have also been chosen to show some failure cases of PressNet.

Observing the foot pressure heatmaps in columns of KNN, PressNet-V1 and PressNet-V2, it is evident that the heatmaps generated by PressNET-V2 are more similar to Ground truth heatmaps when compared to the other two. This is supported by the mean absolute frame errors of the

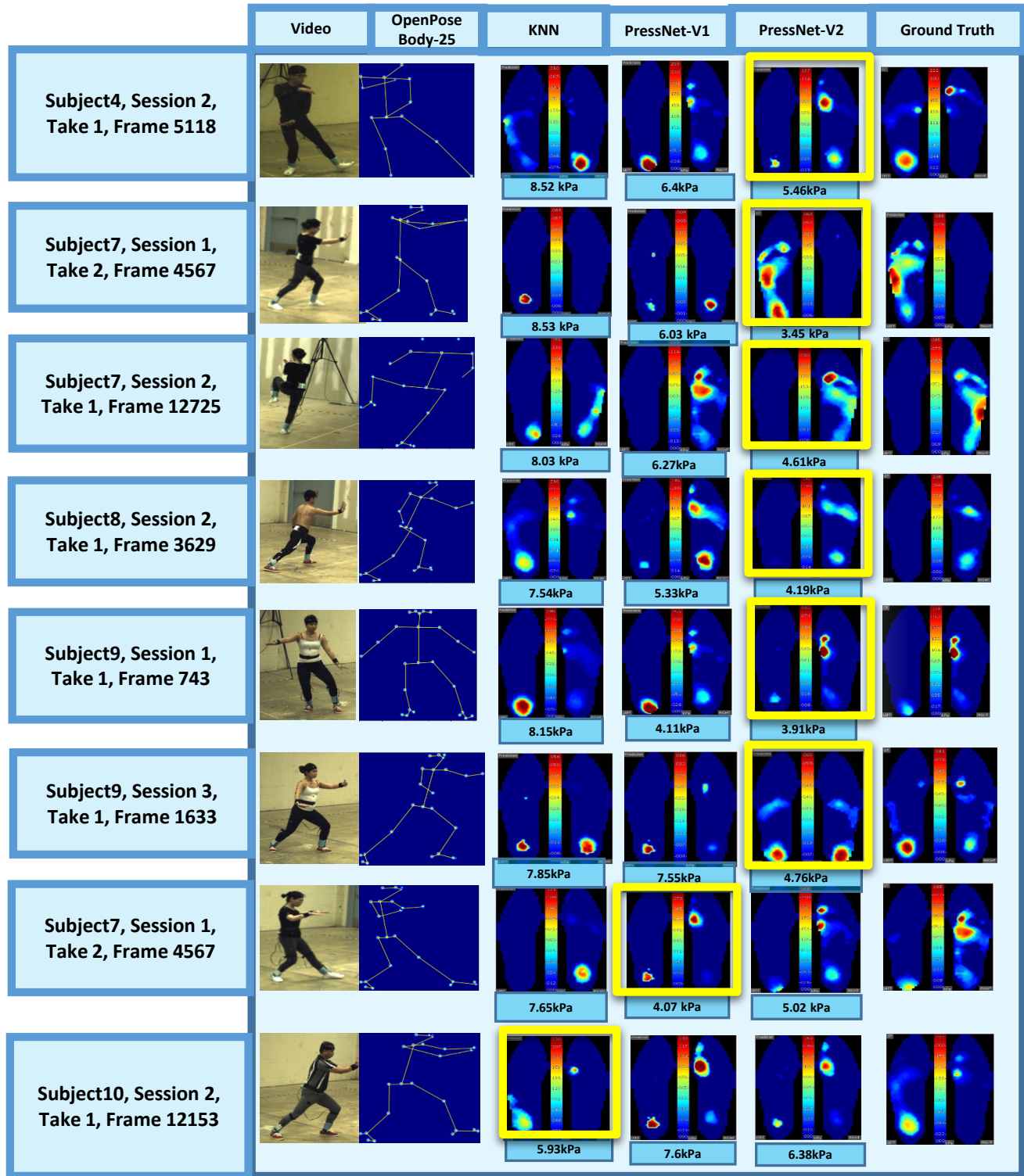


Figure 5. Qualitative results showing (Left to Right): Input data, Ground truths and Predictions from KNN, PressNet-V1 and PressNet-V2. The footpressure prediction with the lowest mean absolute error is shown with a yellow rectangle around it.

networks. KNN results are visually very poor when compared to the two PressNets. This is because KNN is merely picking the frame with the shortest distance between joints in a cross-subject evaluation. As the style of performance and body dynamics differs for each subject, KNN is unable to generalize to a change in subjects, leading to the highest mean absolute error among the three.

Different poses can lead to the same foot pressure. Consider Frames 5,118 of Subject 4, Session 2 (first row), Take 1 and 12,153 of Subject 10, Session 2, Take 1 (last row). They have similar foot pressure heatmaps, with the left heel and the right fore foot having a high pressure intensity, but they correspond to two different poses from two different subjects, the poses from the front view of Subject4 and side view of Subject 10. It can be clearly seen from visualization that PressNET-V2 generates heatmaps with similar pressure intensities as ground truth for both the frames. This shows that our network is able to capture the correlation between joint locations and foot pressure, irrespective of subject, pose, or camera view. Subjects 7 and 9 show the same response, proving that our network is not susceptible to changes in gender, even with different body dynamics and styles.

It can be observed that for Subject 10 in Figure 5, KNN performs better than PressNet. One of the reasons for this might be that the KNN finds a similar pose with a similar foot pressure map in the training data, since multiple poses can lead to the same foot pressure. This frame captures a side view with occluded limbs, thereby increasing the error in OpenPose estimation. This hypothesis is supported by zero confidences for four joints, leading to a worse mean absolute error on PressNet-V1 and PressNet-V2.

5. Summary and Conclusion

In this paper, we explore the feasibility of detecting foot pressure from 2D joint detection in video. This is the first work in an effort to bring human body dynamics into the computer vision community. We demonstrate, both quantitatively and qualitatively the effectiveness of our PressNET networks on a unique dataset. We compare with a standard K-Nearest Neighbor method to validate that our networks are learning foot pressures compared with a standard baseline method with statistical significance.

We hope to extend this work to start focusing on more aspects of human body dynamics such as regressing directly to muscle and weight distributions, balance, and force. Our overarching goal will be to estimate all human body dynamics and validate them using bio-mechanically validated data (rather than close approximations of human labelers), to try and create a new type of problem for computer vision going beyond the basic human joint/pose detection to a more colorful and challenging problem of detecting human body dynamics.

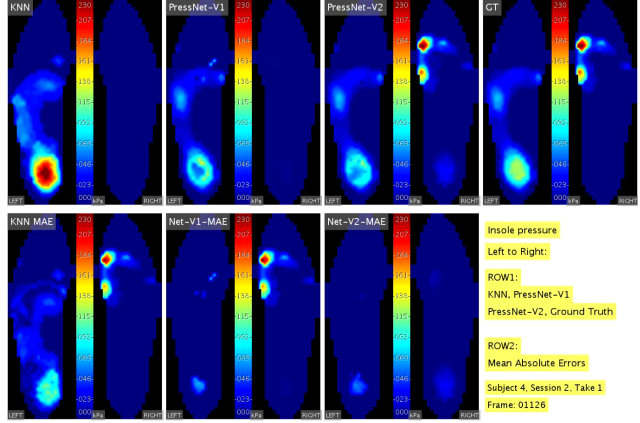


Figure 6. Screenshot from the video rendered from Take 1 of Session 2 from Subject 4. Left to Right: Row 1: KNN Prediction, PressNet-V1 Prediction, PressNet-V2 Prediction, Ground Truth. Row 2: KNN MAE, PressNet-V1 MAE, PressNet-V2 MAE, Information Sub-frame

6. Supplementary Material

6.1. Qualitative Evaluation by Visualization

In this section, we emphasize on qualitative evaluation of our results (Table 3, Section 4 in our main paper) by visualization of foot pressure outputs obtained from K-Nearest Neighbors (KNN), PressNet-V1 and PressNet-V2. We consolidate the predictions of our networks, predictions of KNN baseline and the Ground truth foot pressures for a single take of a session from a subject into a video. The video features the change in foot pressure during a performance. The network predictions can be visually compared with Ground Truths and KNN baseline for a particular frame. We use Mean Absolute Error as a metric for quantitative analysis in the paper. In the videos, we show the mean absolute error as the absolute difference heatmap between the network outputs and ground truth foot pressures. This enables visual realization of error in foot pressure for a particular frame. Figure 6 shows a screen shot of the video, rendered using data from Take 1 of Session 2 from Subject 4. Each video frame has 8 sub-frames. Sub-frames in row 1, from left to right, portray predictions from KNN, PressNet-V1, PressNet-V2 and Ground Truths. Under each prediction, in row 2, corresponding absolute difference heatmaps with respect to ground truth foot pressure are shown. The last sub-frame in row 2 provides information about the video frame.

Test Subject	Number of frames	Video Length (Minutes.Seconds)	File Name
4	14248	04.44	Subject-4-FootPressureVideo.mp4
7	17354	05.54	
8	14103	04.42	Subject-8-FootPressureVideo.mp4
9	11294	03.45	Subject-9-FootPressureVideo.mp4
10	14500	05.09	Subject-10-FootPressureVideo.mp4

Table 5. Number of frames of prediction data used from Session 2, Take 1 of every subject and corresponding video lengths

The predictions, ground truths and absolute difference heatmaps are rendered on the same color scale for the entire video at 50 fps. The color bar in each sub-frame represents foot pressure intensity in kilo-Pascals (kPa). It starts from a shade of blue, representing 0 foot pressure to a dark shade of red, corresponding to the maximum foot pressure during the performance. The colors in between represent different levels of pressure intensities between 0 and the maximum. The videos are rendered in .mp4 format and compressed to H.264 codec. We submit videos of four subjects - Subject4, Subject8, Subject9 and Subject10 due to the 100MB limit on submitted documents. Data for each video is taken from Take 1 of Session 2 of every subject. Table 6.1 lists the number of frames in each video along with the corresponding video lengths that have been uploaded. It can be visually observed that PressNet-V2 performs the best, as portrayed in the paper, followed by PressNet-V1. Overall, both the networks show a better qualitative and quantitative performance when compared to KNN.

Figures 7 to 10 show a sample video frames along with the corresponding input Tai Chi video frames and open pose joint heatmaps for subjects 4, 8, 9 and 10 respectively. Best prediction in each sample has a yellow bounding box around it.

6.2. Center of Pressure

In our paper, we emphasize on human gait stability analysis as the motivation to our work. With stability analysis, we can understand complex mechanisms of the human postural system, which contribute to the development of efficient solutions for unstable postures in terms of orientation and equilibrium. Any human activity comprises of four main tasks: Initiation and termination of a locomotion movement, generation of a continuous movement, maintenance of the equilibrium and adaptability to meet changes in the environment. [10, 15, 19, 20, 21, 24, 26, 28, 29, 37, 39, 49, 50] Maintenance of equilibrium is crucial in determining the stability of human gait during a physical activity such as walking, running, dancing, jumping, playing sports etc. for two reasons: First, the center of mass is located at a considerable distance from the support area. Second, for a major period during any of the physical activities mentioned above, the body is supported by a single limb with the center of mass outside the base of the support area. The Support area in the single support phase is approximately equal to the area of a single foot. In the double support phase, the area is much wider and becomes a convex hull of two-foot areas.

6.2.1 CoP Evaluation

There are two main criteria that can be employed to study stability of human gait: Zero Moment Point (ZMP) and

Ground Projection of Center of Mass (GCOM). [?] GCOM criteria is the projection of center of gravity onto the Base of Support (BoS) shown in Figure 11. It states that a human gait is statistically stable if the gravity line from its center of mass falls within BoS, also called the support polygon. [26]. If GCOM point is beyond the support polygon, it is equivalent to the presence of an uncompensated moment acting on the foot, which causes it to rotate around the point on the polygon boundary resulting in instability. ZMP is a point where the total moment generated due to gravity and inertia equals zero. For stability, the ZMP must be inside BoS. ZMP is also called as the Center Of Pressure (CoP). Figure 11 shows a diagram of foot pressure annotated with the CoP, shown as a red star, relative to the pressure from both feet shown as regions color-coded from low pressure (yellow) to moderate pressure (red) to high pressure (brown). As shown in this figure, CoP is the ground reaction force and CoM/CoG is the opposing force. Larger distance (euclidean/absolute) between the two 2D points indicates reduced stability. We use Euclidean distance/Mean Squared Error between CoM and CoP as a quantitative metric, which can be used for stability analysis.

Calculation of Center of Pressure relies on foot position, orientation and pressure data. CoP is calculated as the weighted mean of all the foot pressure in the XY (ground) plane. Our dataset records spatio-temporally registered foot position and orientation using motion capture. This accurate foot position and orientation data is used consistently with each foot pressure frame (KNN, PressNet-V2 and Ground Truth) to calculate CoP.

6.2.2 Quantitative Evaluation

KNN Test Subject	2D CoP Euclidean Error (mm)				
	Mean	Std	Median	Max	Min
4	196.87	198.83	122.93	1136.4	0
7	163.97	157.94	103	699.76	0
8	216.16	222.78	123.61	1067	0
9	191.56	200.92	111.36	902.73	0
10	179.1	173.1	116.98	971.52	0

PressNET V2 Test Subject	2D CoP Euclidean Error(mm)				
	Mean	Std	Median	Max	Min
4	66.18	116.78	26.51	1179	0
7	52.36	83.64	23.09	682.72	0
8	70.98	119.9	30.59	1048.1	0
9	61.83	109.9	20.76	888.11	0
10	59.25	95.67	25.51	759.82	0

Table 6. Table of 2D CoP Euclidean Error (Euclidean distance from Ground Truth) for KNN and PressNet-V2

Here, we emphasize on using the results from our networks to calculate errors in CoP for the sequences of Tai

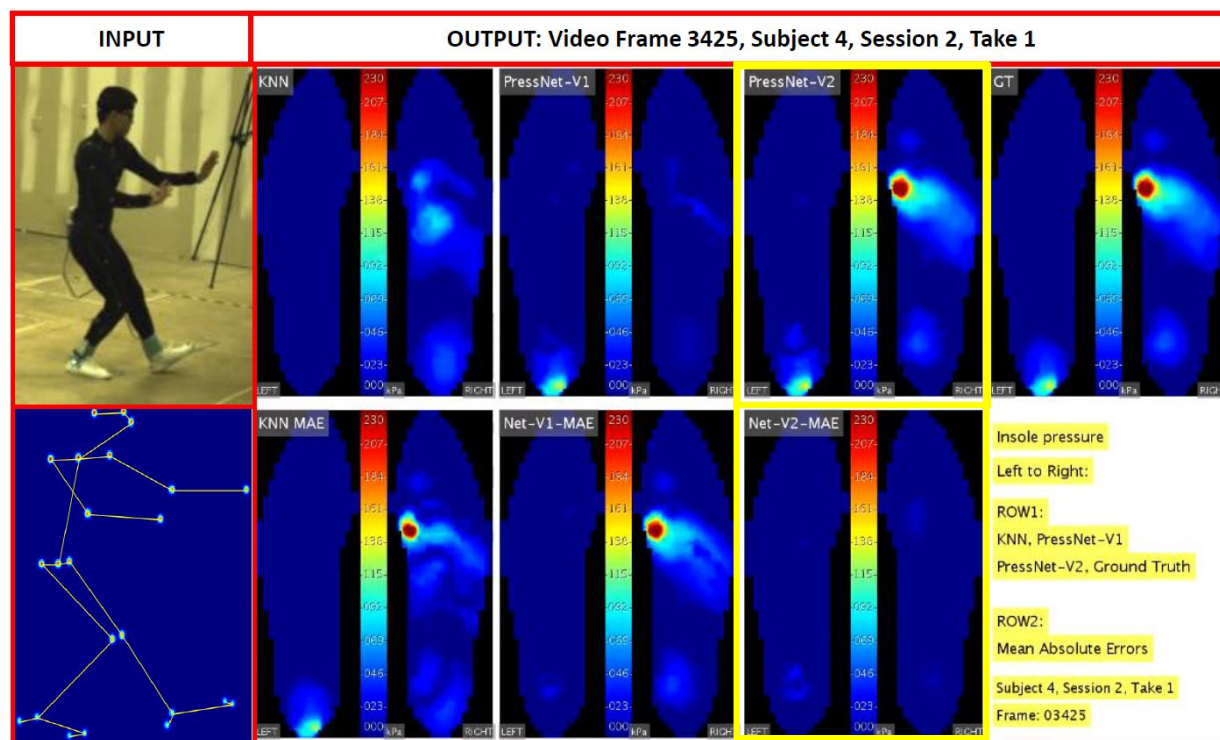


Figure 7. Qualitative results showing (Left to Right): Input data, Video Frame 3425 from Subject 4, Session 2, Take 1. Best prediction has a yellow bounding box around it.

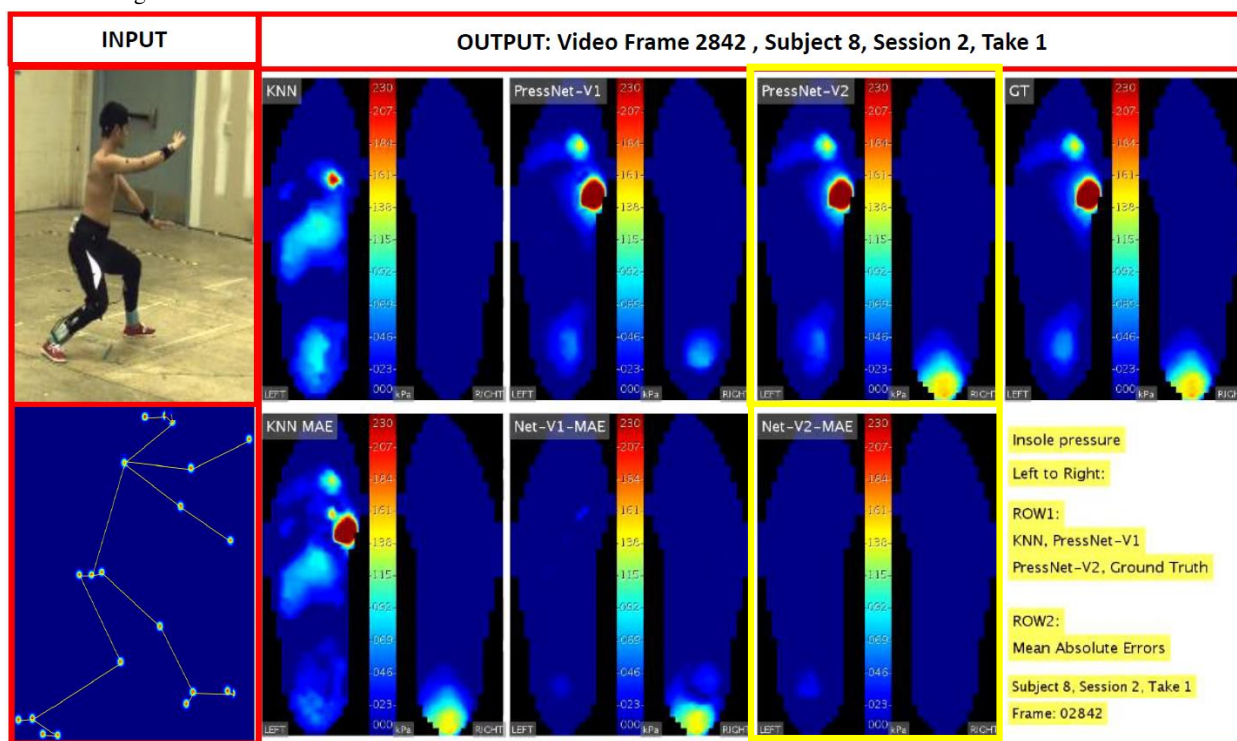


Figure 8. Qualitative results showing (Left to Right): Input data, Video Frame 2842 from Subject 8, Session 2, Take 1. Best prediction has a yellow bounding box around it.

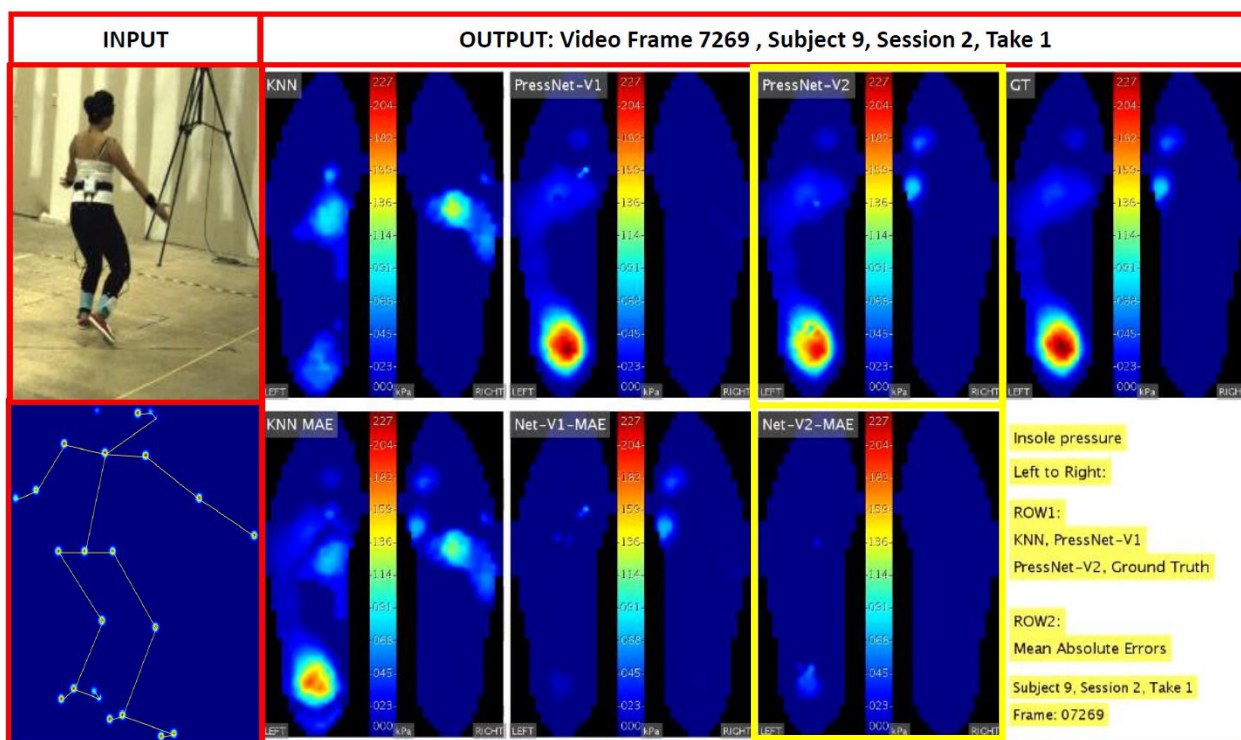


Figure 9. Qualitative results showing (Left to Right): Input data, Video Frame 7269 from Subject 9, Session 2, Take 1. Best prediction has a yellow bounding box around it.

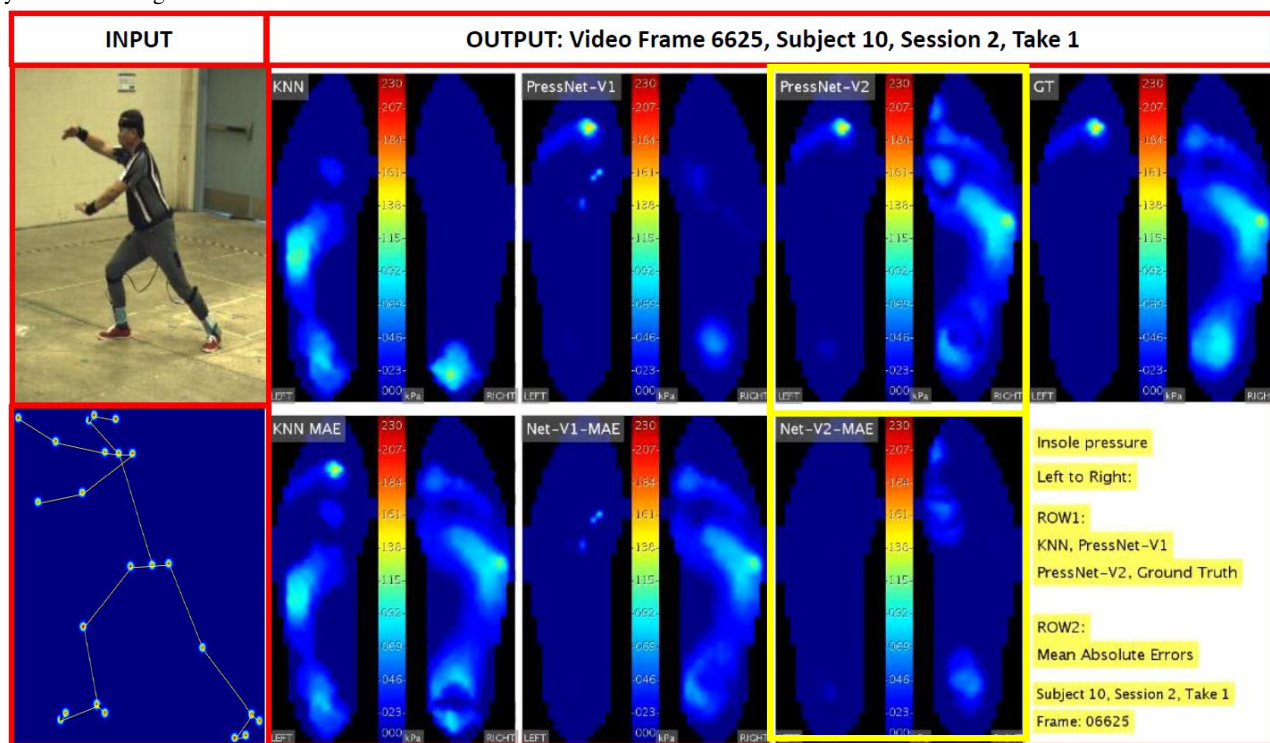


Figure 10. Qualitative results showing (Left to Right): Input data, Video Frame 6625 from Subject 10, Session 2, Take 1. Best prediction has a yellow bounding box around it.

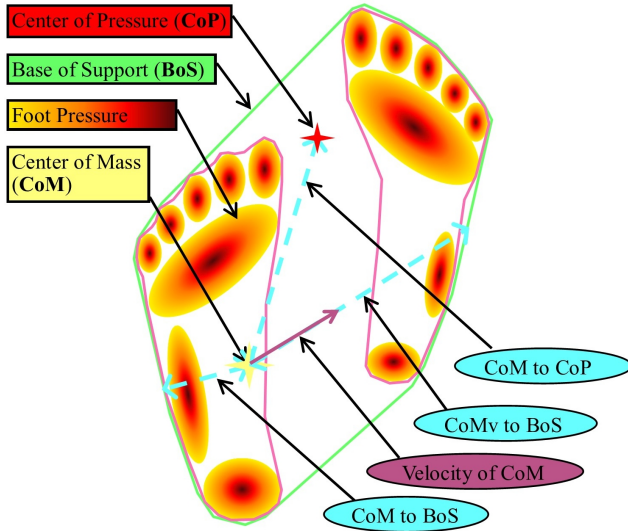


Figure 11. Stability Components for CoP measurements

Chi performances considered in Section 6.1, along with Subject-7. Since PressNet-V2 had the least mean absolute error, we have calculated CoP using the outputs of this network, compared with CoP of KNN baseline. Euclidean distance (square root of Mean Squared error) is chosen to calculate the 2D error between ground truth and our models. Table 6 lists the Euclidean errors in CoP for KNN and PressNet-V2. PressNet-V2 has significantly lower errors for all subjects, making it a better tool for human gait stability analysis. Figure 12 shows the 2D CoP Euclidean errors for Subjects 4,7,8,9 and 10. It can be observed from the figures that the spread of errors of CoP is significantly lower when compared to that of KNN.

From Table 6, it is evident that the median errors for PressNet-V2 are approximately 3 times lesser than that of KNN. The distribution of euclidean errors are concentrated around zero millimeters, showing that the accuracy of CoP calculations are significantly better than KNN, with lesser variance. Thus, we have successfully developed a deep learning framework for human gait stability analysis by regressing foot pressure from video.

References

- [1] A. Agarwal and B. Triggs. 3d human pose from silhouettes by relevance vector regression. In *null*, pages 882–888. IEEE, 2004. 2
- [2] S. J. Allen, M. A. King, and M. R. Yeadon. Is a single or double arm technique more advantageous in triple jumping? *Journal of biomechanics*, 43(16):3156–3161, 2010. 1
- [3] C. M. Bishop et al. *Neural networks for pattern recognition*. Oxford university press, 1995. 2, 5
- [4] F. Bogo, A. Kanazawa, C. Lassner, P. Gehler, J. Romero, and M. J. Black. Keep it smpl: Automatic estimation of 3d human pose and shape from a single image. In *European Conference on Computer Vision*, pages 561–578. Springer, 2016. 2
- [5] A. Bulat and G. Tzimiropoulos. Human pose estimation via convolutional part heatmap regression. In *European Conference on Computer Vision*, pages 717–732. Springer, 2016. 1
- [6] Z. Cao, T. Simon, S.-E. Wei, and Y. Sheikh. Real-time multi-person 2d pose estimation using part affinity fields. *arXiv preprint arXiv:1611.08050*, 2016. 1, 3
- [7] C.-H. Chen and D. Ramanan. 3d human pose estimation= 2d pose estimation+ matching. In *CVPR*, volume 2, page 6, 2017. 1
- [8] W. Chen, H. Wang, Y. Li, H. Su, Z. Wang, C. Tu, D. Lischinski, D. Cohen-Or, and B. Chen. Synthesizing training images for boosting human 3d pose estimation. In *3D Vision (3DV), 2016 Fourth International Conference on*, pages 479–488. IEEE, 2016. 1
- [9] X. Chen and A. L. Yuille. Articulated pose estimation by a graphical model with image dependent pairwise relations. In *Advances in neural information processing systems*, pages 1736–1744, 2014. 1
- [10] I.-K. Chiang, I. Spiro, S. Lee, A. Lees, J. Liu, C. Bregler, and Y. Liu. Dancing with turks. In *Proceedings of the 23rd ACM international conference on Multimedia*, pages 241–250. ACM, 2015. 2, 9
- [11] Z. J. Domire and J. H. Challis. Maximum height and minimum time vertical jumping. *Journal of biomechanics*, 48(11):2865–2870, 2015. 1
- [12] X. Fan, K. Zheng, Y. Lin, and S. Wang. Combining local appearance and holistic view: Dual-source deep neural networks for human pose estimation. In *Proceedings of the IEEE Conference on Computer Vision and Pattern Recognition*, pages 1347–1355, 2015. 1, 5
- [13] S. R. Goldberg, S. Öunpuu, and S. L. Delp. The importance of swing-phase initial conditions in stiff-knee gait. *Journal of biomechanics*, 36(8):1111–1116, 2003. 2
- [14] I. Goodfellow, J. Pouget-Abadie, M. Mirza, B. Xu, D. Warde-Farley, S. Ozair, A. Courville, and Y. Bengio. Generative adversarial nets. In *Advances in neural information processing systems*, pages 2672–2680, 2014. 4
- [15] A. Goswami. Foot rotation indicator (fri) point: A new gait planning tool to evaluate postural stability of biped robots. In *Robotics and Automation*, 1999.

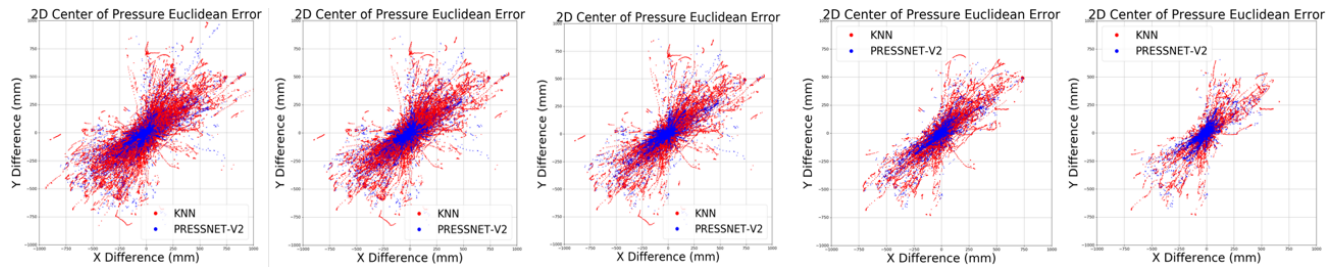


Figure 12. Left to Right: 2D CoP Euclidean Error Plots for Subject: 4, 7, 8, 9, 10

- Proceedings. 1999 IEEE International Conference on*, volume 1, pages 47–52. IEEE, 1999. 2, 9
- [16] R. A. Güler, G. Trigeorgis, E. Antonakos, P. Snape, S. Zafeiriou, and I. Kokkinos. Densereg: Fully convolutional dense shape regression in-the-wild. In *CVPR*, volume 2, page 5, 2017. 1
- [17] I. Gulrajani, F. Ahmed, M. Arjovsky, V. Dumoulin, and A. C. Courville. Improved training of wasserstein gans. In *Advances in Neural Information Processing Systems*, pages 5767–5777, 2017. 4
- [18] F. Han, B. Reily, W. Hoff, and H. Zhang. Space-time representation of people based on 3d skeletal data: A review. *Computer Vision and Image Understanding*, 158:85–105, 2017. 2
- [19] A. L. Hof. The equations of motion for a standing human reveal three mechanisms for balance. *Journal of biomechanics*, 40(2):451–457, 2007. 2, 9
- [20] A. L. Hof. The extrapolated center of mass concept suggests a simple control of balance in walking. *Human movement science*, 27(1):112–125, 2008. 2, 9
- [21] E. Hsu, K. Pulli, and J. Popović. Style translation for human motion. In *ACM Transactions on Graphics (TOG)*, volume 24, pages 1082–1089. ACM, 2005. 9
- [22] M. A. Hughes, B. S. Myers, and M. L. Schenkman. The role of strength in rising from a chair in the functionally impaired elderly. *Journal of biomechanics*, 29(12):1509–1513, 1996. 2
- [23] S. Ioffe and C. Szegedy. Batch normalization: Accelerating deep network training by reducing internal covariate shift. *arXiv preprint arXiv:1502.03167*, 2015. 5
- [24] Y.-S. Jeong, M. K. Jeong, and O. A. Omitaomu. Weighted dynamic time warping for time series classification. *Pattern Recognition*, 44(9):2231–2240, 2011. 2, 9
- [25] A. Kanazawa, M. J. Black, D. W. Jacobs, and J. Malik. End-to-end recovery of human shape and pose. *A-1 A-2 A-3 A-4 A-5 A-6 A-7*, 2017. 2
- [26] E. J. Keogh and M. J. Pazzani. Derivative dynamic time warping. In *Proceedings of the 2001 SIAM International Conference on Data Mining*, pages 1–11. SIAM, 2001. 9
- [27] J. H. Ko, Z. Wang, J. H. Challis, and K. M. Newell. Compensatory mechanisms of balance to the scaling of arm-swing frequency. *Journal of biomechanics*, 48(14):3825–3829, 2015. 2
- [28] K. Kulkarni, G. Evangelidis, J. Cech, and R. Horaud. Continuous action recognition based on sequence alignment. *International Journal of Computer Vision*, 112(1):90–114, 2015. 9
- [29] W. Land, D. Volchenkov, B. E. Bläsing, and T. Schack. From action representation to action execution: exploring the links between cognitive and biomechanical levels of motor control. *Frontiers in computational neuroscience*, 7:127, 2013. 9
- [30] H.-J. Lee, C. Zen, et al. Determination of 3d human-body postures from a single view. *Computer Vision Graphics and Image Processing*, 30(2):148–168, 1985. 2
- [31] J. Martinez, R. Hossain, J. Romero, and J. J. Little. A simple yet effective baseline for 3d human pose estimation. In *International Conference on Computer Vision*, volume 1, page 5, 2017. 2
- [32] F. Moreno-Noguer. 3d human pose estimation from a single image via distance matrix regression. In *Computer Vision and Pattern Recognition (CVPR), 2017 IEEE Conference on*, pages 1561–1570. IEEE, 2017. 2
- [33] J. Mrozowski, J. Awrejcewicz, and P. Bamberiski. Analysis of stability of the human gait. *Journal of theoretical and applied mechanics*, 45(1):91–98, 2007. 2
- [34] V. Nair and G. E. Hinton. Rectified linear units improve restricted boltzmann machines. In *Proceedings of the 27th international conference on machine learning (ICML-10)*, pages 807–814, 2010. 5
- [35] A. Newell, K. Yang, and J. Deng. Stacked hour-glass networks for human pose estimation. In *Euro*

- pean Conference on Computer Vision, pages 483–499. Springer, 2016. 1, 2
- [36] B. X. Nie, P. Wei, and S.-C. Zhu. Monocular 3d human pose estimation by predicting depth on joints. In *IEEE International Conference on Computer Vision*, 2017. 2
- [37] Y.-C. Pai. Movement termination and stability in standing. *Exercise and sport sciences reviews*, 31(1):19–25, 2003. 2, 9
- [38] V. Parameswaran and R. Chellappa. View independent human body pose estimation from a single perspective image. In *Computer Vision and Pattern Recognition, 2004. CVPR 2004. Proceedings of the 2004 IEEE Computer Society Conference on*, volume 2, pages II–II. IEEE, 2004. 2
- [39] T. C. Pataky, T. Mu, K. Bosch, D. Rosenbaum, and J. Y. Goulermas. Gait recognition: highly unique dynamic plantar pressure patterns among 104 individuals. *Journal of The Royal Society Interface*, 9(69):790–800, 2012. 2, 9
- [40] G. Pavlakos, X. Zhou, K. G. Derpanis, and K. Daniilidis. Coarse-to-fine volumetric prediction for single-image 3d human pose. In *Computer Vision and Pattern Recognition (CVPR), 2017 IEEE Conference on*, pages 1263–1272. IEEE, 2017. 2
- [41] G. Pavlakos, X. Zhou, K. G. Derpanis, and K. Daniilidis. Coarse-to-fine volumetric prediction for single-image 3d human pose. In *Computer Vision and Pattern Recognition (CVPR), 2017 IEEE Conference on*, pages 1263–1272. IEEE, 2017. 2
- [42] G. Rogez, P. Weinzaepfel, and C. Schmid. Lcr-net++: Multi-person 2d and 3d pose detection in natural images. *arXiv preprint arXiv:1803.00455*, 2018. 2
- [43] J. Scott, R. T. Collins, C. Funk, and Y. Liu. 4d model-based spatiotemporal alignment of scripted taiji quan sequences. In *ICCV Workshops*, pages 795–804, 2017. 2
- [44] E. Simo-Serra, A. Ramisa, G. Alenyà, C. Torras, and F. Moreno-Noguer. Single image 3d human pose estimation from noisy observations. In *Computer Vision and Pattern Recognition (CVPR), 2012 IEEE Conference on*, pages 2673–2680. IEEE, 2012. 2
- [45] X. Sun, J. Shang, S. Liang, and Y. Wei. Compositional human pose regression. In *The IEEE International Conference on Computer Vision (ICCV)*, volume 2, page 7, 2017. 2
- [46] D. Tome, C. Russell, and L. Agapito. Lifting from the deep: Convolutional 3d pose estimation from a single image. *CVPR 2017 Proceedings*, pages 2500–2509, 2017. 2
- [47] J. J. Tompson, A. Jain, Y. LeCun, and C. Bregler. Joint training of a convolutional network and a graphical model for human pose estimation. In *Advances in neural information processing systems*, pages 1799–1807, 2014. 2
- [48] A. Toshev and C. Szegedy. Deeppose: Human pose estimation via deep neural networks. In *Proceedings of the IEEE conference on computer vision and pattern recognition*, pages 1653–1660, 2014. 1
- [49] R. Vera-Rodriguez, J. S. Mason, J. Fierrez, and J. Ortega-Garcia. Comparative analysis and fusion of spatiotemporal information for footprint recognition. *IEEE transactions on pattern analysis and machine intelligence*, 35(4):823–834, 2013. 2, 9
- [50] J. Zhao and L. Itti. shapedtw: shape dynamic time warping. *arXiv preprint arXiv:1606.01601*, 2016. 9
- [51] X. Zhou, Q. Huang, X. Sun, X. Xue, and Y. Wei. Towards 3d human pose estimation in the wild: a weakly-supervised approach. In *IEEE International Conference on Computer Vision*, 2017. 2
- [52] X. Zhou, X. Sun, W. Zhang, S. Liang, and Y. Wei. Deep kinematic pose regression. In *European Conference on Computer Vision*, pages 186–201. Springer, 2016. 2
- [53] X. Zhou, M. Zhu, S. Leonardos, K. G. Derpanis, and K. Daniilidis. Sparseness meets deepness: 3d human pose estimation from monocular video. In *Proceedings of the IEEE conference on computer vision and pattern recognition*, pages 4966–4975, 2016. 2